

A Ring-like Zone of Strong Radial Gas Motions in the Disk of NGC 6181 ^{*}

O. K. Sil'chenko¹, A. V. Zasov¹, A. N. Burenkov², and J. Boulesteix³

¹ Sternberg Astronomical Institute, University av. 13, Moscow 119899, Russia

² Special Astrophysical Observatory, Nizhnij Arkhyz, Karachaj-Cherkess Republic, 357147 Russia

³ Observatoire de Marseille, 2 Place Le Verrier, F-13248 Marseille Cedex 04, France

November 18, 2018

Abstract. The Sc galaxy NGC 6181 was observed at the 6m telescope of SAO RAS with the scanning Perot-Fabry interferometer in the H α emission line and at the 1m telescope of SAO RAS in *BVRI* broadband filters with CCD. Subtraction of the mean circular rotation curve from the two-dimensional velocity field has revealed a ring-like zone with a diameter about of 2 kpc where strong radial gas motions are present. The form of the ring is almost perfectly circular in the plane of the galaxy. It is located closer to the center than the beginning of the well-defined spiral structure, but outside of the central bulge-dominated region. The detected radial velocity reduced to the plane of the galaxy is about 100 km · s⁻¹ and probably is azimuthally dependent. The very inner region of the galaxy, $r < 3''$ or 0.5 kpc, shows a turn of the dynamical major axis by about 30°. Central continuum isophotes are also twisted which suggests the presence of small nuclear bar .

Key words: Galaxies: spirals, kinematics - Scanning Perot-Fabry interferometry

cross-sections of the galaxy and found line-of-sight velocity distributions to be quite asymmetrical. They concluded that NGC 6181 is not an axisymmetric galaxy being intermediate between a barred and a normal spiral. The form of thin dust lanes in the center of NGC 6181 gave some support to this hypothesis. In addition, they noted that "the structural center of the galaxy is not the center of the velocity distribution", because the systemic velocities determined from the outer and the inner parts of line-of-sight velocity curves disagreed.

Our group (Afanasiev et al. 1992) has repeated a long-slit kinematical study of NGC 6181 at the 6m telescope of the Special Astrophysical Observatory (SAO RAN) and fully confirmed the unusual asymmetrical character of the one-dimensional line-of-sight velocity distributions. It has been proposed that it is the southern part of the galaxy which reveals strong non-circular gas motions up to distances of about 20'' from the center. But it became evident that the obtaining of the two-dimensional velocity field is necessary to clarify the situation.

Table 1. Global parameters of NGC 6181

Hubble type	SAB(rs)c
R_{25}	12.3 kpc
B_T^0	11.7
M_B	-20.93
$V_r(\text{radio})$	2374 km · s ⁻¹
$V_{gal.std-of-rest}$	2492 km · s ⁻¹
Distance	33.6 Mpc ($H_0=75 \text{ km} \cdot \text{s}^{-1} \cdot \text{Mpc}^{-1}$)
Inclination	66.6°
MA_{phot}	175°

1. Introduction

NGC 6181 is an isolated late-type giant spiral galaxy whose high surface brightness of gas emission and inclination of about 60° are favorable for a detailed kinematical study. Global parameters of the galaxy are listed in Table 1 being taken basically from LEDA (Lyon-Meudon Extragalactic Database). The first kinematical investigation of NGC 6181 was undertaken nearly 30 years ago by Burbidge et al. (1965). They obtained three spectral long-slit

Send offprint requests to: O. K. Sil'chenko

^{*} Based on observations collected with the 6m telescope at the Special Astrophysical Observatory (SAO) of the Russian Academy of Sciences (RAS).

2. Observations

The two-dimensional velocity field of NGC 6181 was obtained at the 6m telescope on September 24, 1993. The scanning Perot-Fabry interferometer was installed inside of the pupil plane of a focal reducer which was attached to the F/4 prime focus of the telescope. An intensified photon counting system (IPCS) 512×512 was used as the detector. Instrument parameters are given in Table 2.

Table 2. Scanning Perot-Fabry observations parameters

Input telescope beam	F/4
Output camera beam	F/2.4
Number of pixels	512×512
Pixel scale	$0.35''$
Field	$3' \times 3'$
Filter wavelength	$\lambda_f=6620 \text{ \AA}$
Filter FWHM	10 \AA
Galaxy H_α wavelength	$\lambda_g=6615 \text{ \AA}$
Filter transmission at λ_g	35 %
Etalon interference order	501 at 6562.8\AA
Free spectral range at λ_g	$603 \text{ km} \cdot \text{s}^{-1}$
Finesse at λ_g	18
Number of scanned channels	32
Channel step	$18.84 \text{ km} \cdot \text{s}^{-1}$
Number of scanned cycles	7
Basic exposure time	20 s
Total exposure time	4480 s
Calibration line	Neon 6598.98 \AA
Seeing	$< 1.5''$

The "Image-interferometry method" was described in detail earlier (Boulesteix et al. 1983, Amram et al. 1991). Observational data (galaxy and wavelength calibration data) were converted into cubes of 32 images (256×256), with the linear scale being 0.70 arcsec/px and a spectral resolution of about 2–2.5 channels ($40\text{--}50 \text{ km} \cdot \text{s}^{-1}$). A reduction of observational data (correction for phase shifting, subtraction of night-sky emission spectrum, construction of velocity map, a.s.o.) was done by using standard methods, and the Perot-Fabry reducing software ADHOC developed at Marseille Observatory (Boulesteix 1993) was used.

The continuum subtracted H_α image of NGC 6181 (Fig. 1) reveals that the H_α emission is rather strong over the whole galactic disk. So the high quality of the two-dimensional velocity distribution obtained allows to get more detailed information about gas motions in the disk of this galaxy. A sub-cube ($210 \text{ px} \times 185 \text{ px} \times 32 \text{ channels}$), containing the main fraction of H_α emission from the galaxy, was extracted from a reduced data cube. This smaller cube was used for the analysis of the velocity field.

Direct images of NGC 6181 were obtained at the telescope Zeiss-1000 of SAO RAN. Eleven frames of the

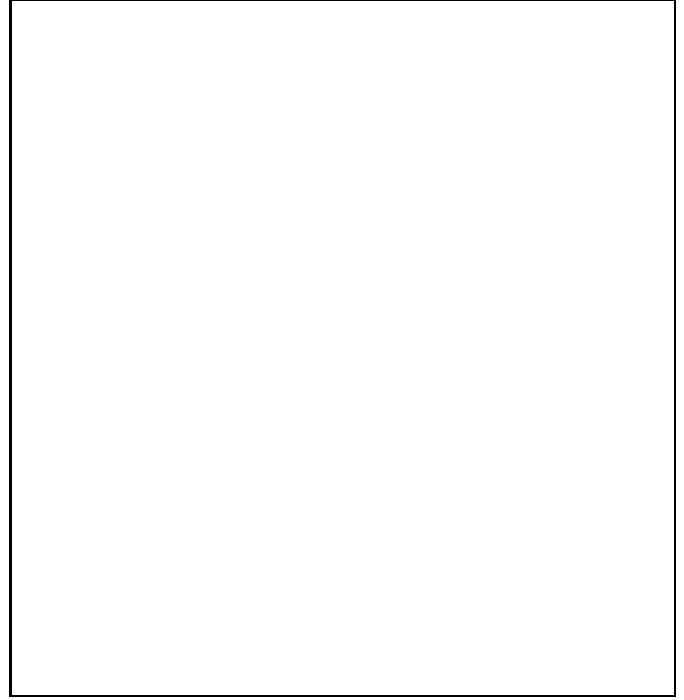


Fig. 1. Monochromatic H_α emission map of NCC 6181. The cross marks the position of the nucleus.

Table 3. Direct image observations

Date	Filter	Exposure time	Zenithal distance
7/8.06.94	<i>I</i>	600 s	49°
7/8.06.94	<i>I</i>	100 s	52°
8/9.06.94	<i>I</i>	600 s	50°
8/9.06.94	<i>R</i>	200 s	52°
8/9.06.94	<i>R</i>	200 s	53°
8/9.06.94	<i>R</i>	200 s	54°
10/11.07.94	<i>B</i>	300 s	57°
10/11.07.94	<i>V</i>	300 s	59°
10/11.07.94	<i>B</i>	300 s	60°
10/11.07.94	<i>V</i>	300 s	61°
10/11.07.94	<i>I</i>	300 s	63°

galaxy have been derived with a CCD camera through the *B*, *V*, *R* and *I* filters of Johnson's system (the log of the observations is given in Table 3). The seeing quality ranged from $2.1''$ (*R* images) to $2.8''$ (*V* and *I* images).

Gray-scaled sky-subtracted *I* and *B* images are presented in Fig. 2a and 2b; flux-calibrated isophotes in *B* ($21.8 \text{ mag/arcsec}^2$ and $25.3 \text{ mag/arcsec}^2$ for the innermost and the outermost isophotes respectively with the step of 0.5 mag/arcsec^2) are shown in Fig.2c. The *B* and *V* frames were calibrated by using 14 aperture photoelectric measurements of NGC 6181 from Burstein et al. (1987). The range of aperture radii is from $16''$ to $48''$. Zero-point magnitudes are obtained with accuracy bet-

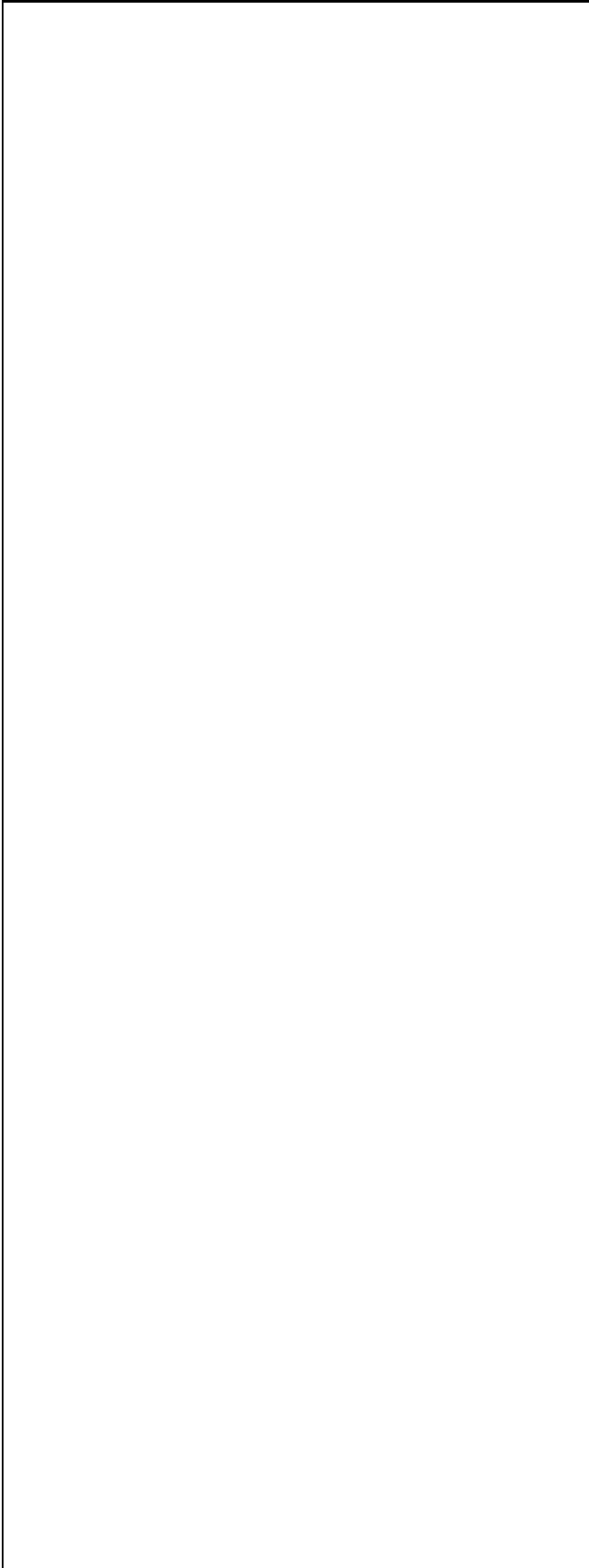


Fig. 2. The I and B images of NGC 6181. The frame is $108'' \times 108''$, north is up and east is to the left.

ter than 0.01 mag, color terms are found to be negligible. The sky brightnesses are estimated as $21.26 \text{ mag/arcsec}^2$ in V and $22.12 \text{ mag/arcsec}^2$ in B ; these values coincide with mean sky brightnesses measured fifteen years ago in the Special Astrophysical Observatory at $z = 60^\circ$ by Neizvestny (1981). To check our BV calibration, we compared multi-aperture photoelectric data for NGC 6181 taken from the catalogue of Longo & Vaucouleurs (1983, 1985) (18 entities excluding old data of PET-54 and BIG-51) with values simulated for the same apertures from our CCD frames. In Fig. 3 one can see a rather good consistency with the photoelectric data, even for large apertures. The calibration of R and I frames was indirect and less precise because standard stars were not observed. Instead $B - V$ colors for five faint stars in the field of the galaxy were measured, and adopting them to be dwarfs we ascribe them mean $V - R$ and $V - I$ colors in accordance with their spectral types (Straizys 1977). The formal accuracy of the calibration constants determined in such a way is 0.12 mag, but we admit a possible systematic shift of our R and I magnitudes by up to 0.3 mag.

3. Photometric properties of NGC 6181

A monochromatic image was constructed from the Perot-Fabry observational data in order to see the morphology of the inner part of NGC 6181. The H_α map of the central part of NGC 6181 (Fig. 1) reveals two bright central sources none of which coincides with the center of the isophotes in the continuum. Two faint tails of H_α emission embrace the central continuum source which is located in the area of very weak emission. Bearing in mind the absence of radio emission from the NGC 6181 nucleus, one may conclude that the nucleus of this galaxy is very quiescent.

The direct images obtained with the 1m telescope were used first of all to find the precise position of the center of the galaxy in the continuum. It was determined with respect to five nearby stars. Location of the center was compared with the H_α distribution and with the dynamical center position (see the next section). In addition we tried to derive some surface brightness distribution characteristics. Fig.2 demonstrates rather smooth image in I , with a weak bar-like disk elongation in the inner part, and a more clumpy image in B ; prominent spiral arms extend up to the outermost radii in all passbands, confirming the grand-design classification of arms made by Elmegreen & Elmegreen (1984).

Fig. 4 presents B and V azimuthally averaged radial surface brightness profiles assuming PA (line of nodes) $=173^\circ$ and inclination 56° in accordance with the velocity field analysis (see below). It shows that this galaxy possesses a very compact bulge which does not affect light distributions beyond the radius $7''$. In the range $12''$ – $25''$ a brightness excess is noticeable over the simple exponential law extrapolated from the outer parts; this excess is repro-

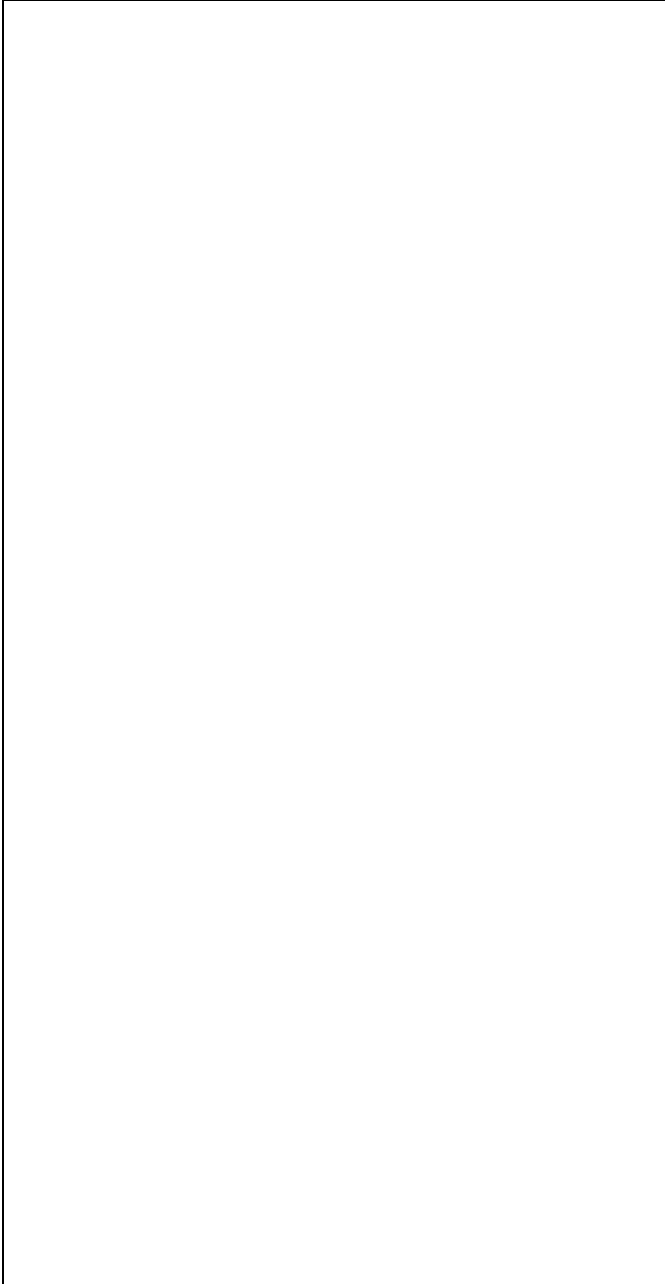


Fig. 3. Comparison of published V and B multi-aperture photoelectric data on NGC 6181 and present CCD observations.

duced in all four filters being the largest (0.15 mag) in the B passband. It seems that the radius of $25''$ is a boundary between two disk subsystems. The disk scale measured in the range $25''$ – $45''$ for all four passbands slightly decreases from blue to red (Fig. 5) being in general accordance with earlier results of Elmegreen & Elmegreen (1984) and Roth (1994).

The azimuthally averaged color tends to be bluer up to $r \approx 36''$ and then some reddening occurs, but the slopes of these trends are quite different for different colors (Fig.

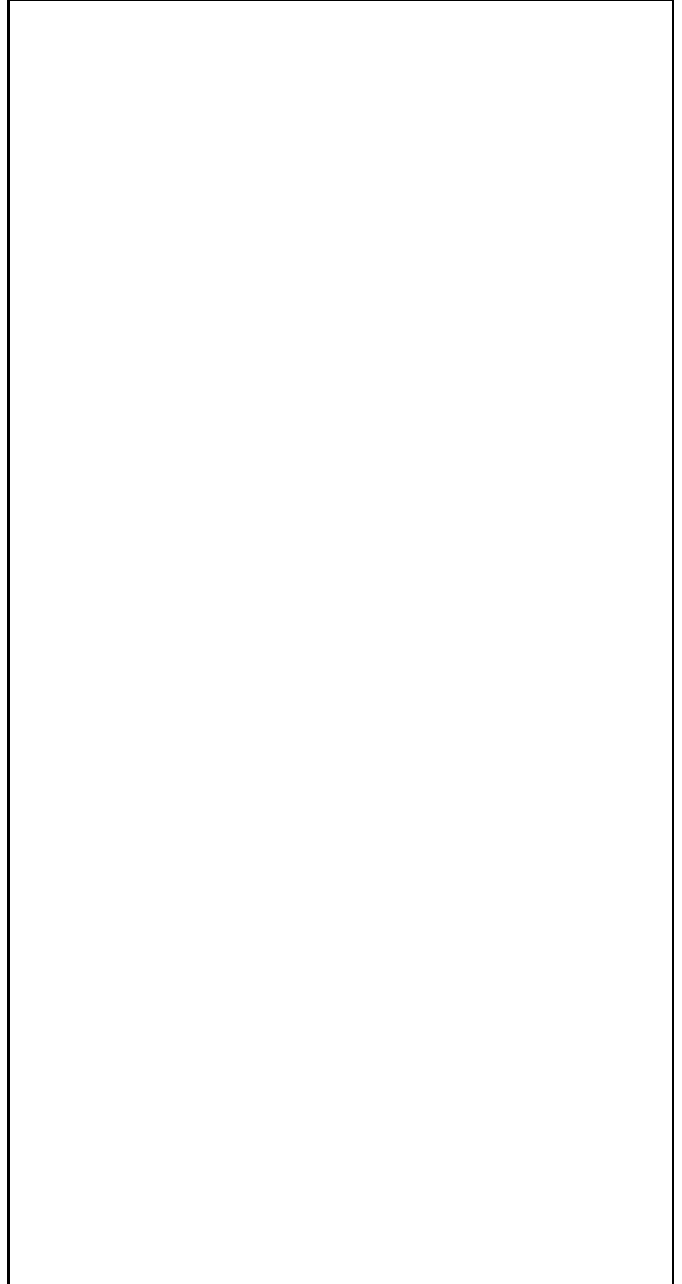


Fig. 4. Radial distributions of azimuthally averaged surface brightness in the B and V passbands. The straight lines represent the disk exponential laws fitted to the radius range of $27''$ to $46''$.

6 and 7). In Fig. 7 we try to compare radial color variations in NGC 6181 with models for old stellar populations showing pure metallicity trend (Worthey 1994) and with a mean observational sequence of galactic colors (Buta & Williams 1995), which is known to be defined mainly by different present-time star formation rate. Color excesses expected due to interstellar reddening in the Galaxy are also shown. The reddening in $B - V$ at $r \approx 5''$ has an azimuthally non-homogeneous character: it is a distinct,

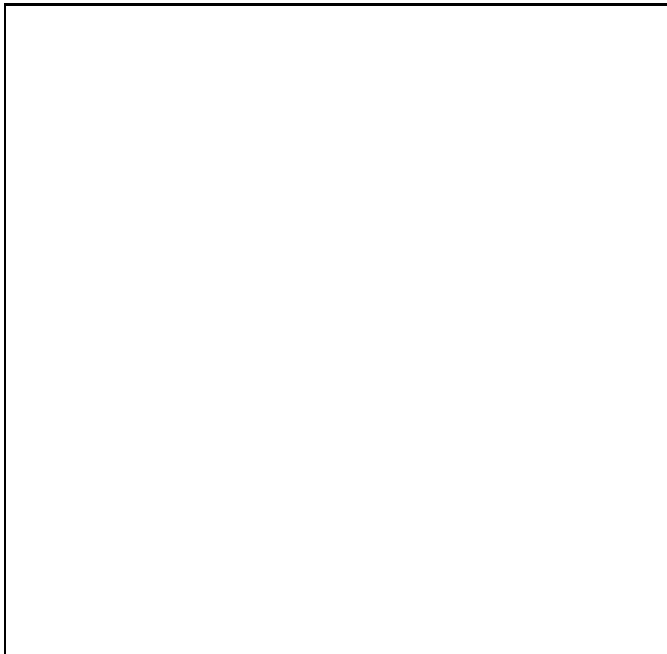


Fig. 5. Disk scale variation with spectral range. Previous published data are also plotted as comparison.

very red spot to the west from the nucleus obviously related to a local dust concentration; the optical characteristics of the dust may be unusual because the spot is absent in $V - R$ and $V - I$ colors. The other color variations seem to be rather azimuthally homogeneous. Comparison of the observed and the expected color trends shows that between the radii $7''$ and $25''$, i. e. in the inner disk distinguished by some brightness excess, the observed color variations may be satisfactorily explained by variations of star formation intensity, because the point grid is roughly parallel to the observational sequence of integrated galactic colors. However the observed color variations in the outer disk are more complicated and rather unusual – especially for $r > 36''$, where the reddening of $B - V$ and $V - R$ occurs under the constant $V - I$. This looks quite inexplicable in the frames of simple effects which influence the color.

The isophote form analysis (pure-ellipse fitting) was carried out to check a possible deviation from axial symmetry. The ellipticity between $1''$ and $7''$ from the center gradually increases from 0.10 (bulge) to 0.35 – a behavior which is quite normal for a galaxy whose inclination is about 60° . The radial dependence of PA_θ is presented in Fig. 8. We see an unambiguous turn of isophotes in the very center of NGC 6181. Measurements in all passbands show that at the radius of $2''$ – $3''$ the position angle of the major axis is $+3^\circ$ with an uncertainty less than 1° , which differs by $\approx 5^\circ$ from the orientation of the outermost isophotes (175° , Nilson 1973; $178.4^\circ \pm 0.5^\circ$, our measurement of the SKYVIEW isophote at the $r = 65''$).



Fig. 6. Color radial profiles averaged over azimuth in the galaxy plane. The r.m.s. error of a single point is less than 0.05 mag

In the radius range $10''$ – $20''$ isophotes are also twisted by $10^\circ - 13^\circ$, but in the opposite sense with respect to the innermost region. Only beyond $r \approx 25''$, where the radial brightness distribution follows a pure exponential law, the isophote major axis becomes aligned with the line of nodes.

4. Velocity field of the ionized gas in NGC 6181

Fig. 9 presents the observed velocity field of NGC 6181. It looks quite regular, with prominent signs of rotation. However in the center of the galaxy a twist of the zero-velocity line is seen which gives evidence for non-circular gas motions in this area in a good agreement with the photometrical data (see below).

A fit of the circular rotation model was made for the full velocity map, with dimensions of 210×185 pixels ($147'' \times 130''$), or within a radius of about $75''$ (12.2 kpc) from the center. Special codes were written for data pro-

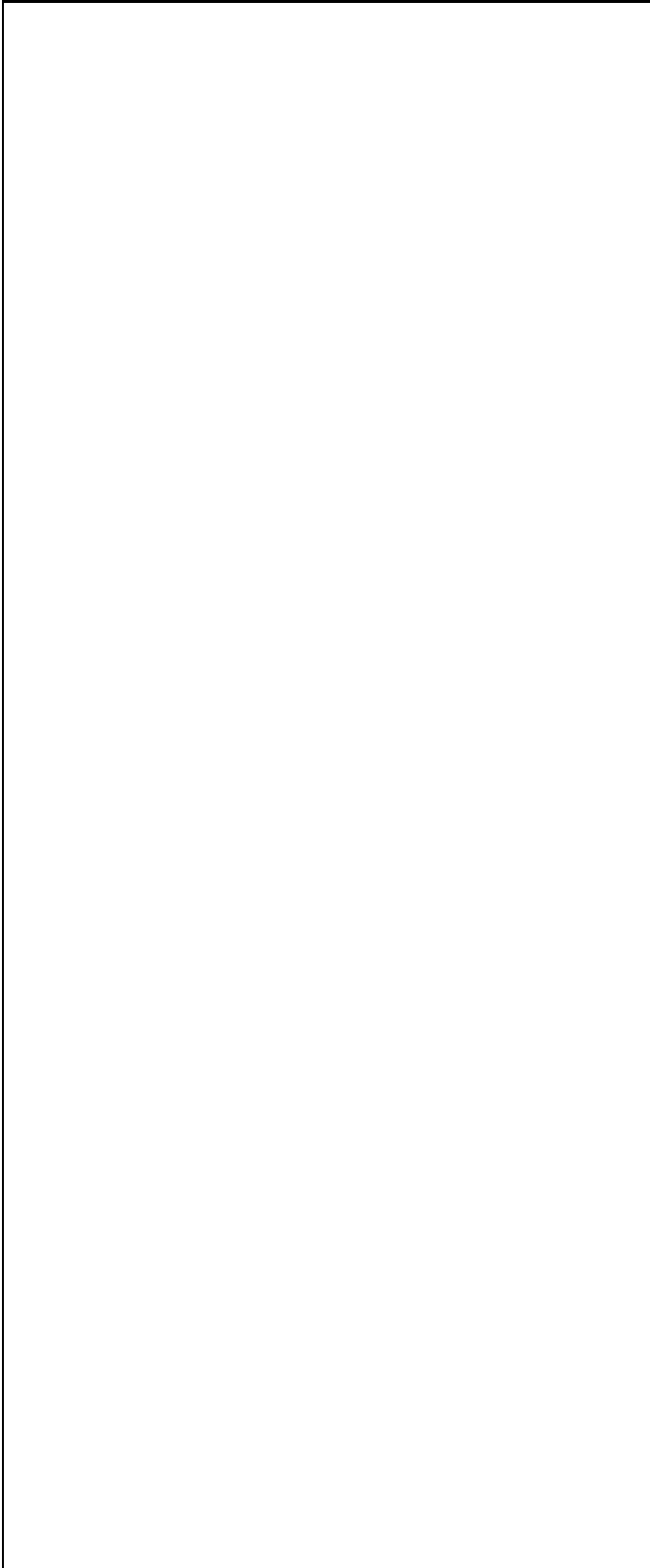


Fig. 7. $(V - R, B - V)$ (a) and $(V - I, B - V)$ (b) diagrams for the radial color variations in NGC 6181. Points are plotted through one arcsecond step. Estimates of $V - R$ and $V - I$ have systematic shift (see the text).

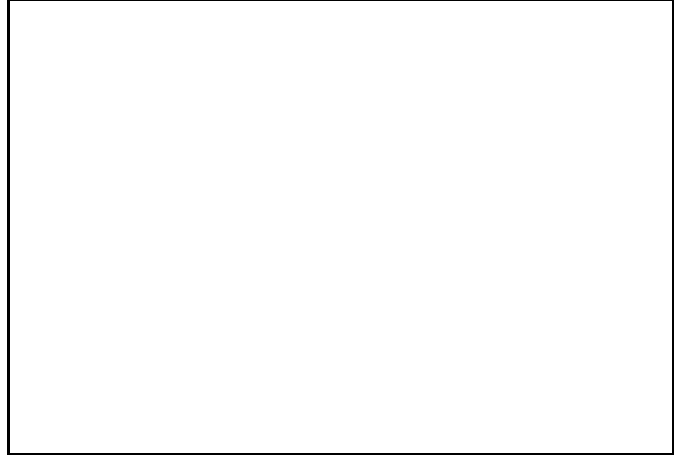


Fig. 8. Variations of the orientation of the photometric major axis along the radius. For $r < 4''$ measurements taken for all passbands were averaged, beyond this radius only I isophotes were used. The long-dashed line indicates the orientation of the outermost isophotes according to our measurement of the SKYVIEW picture, the short-dashed line shows the kinematical line of nodes.

cessing. The galactic disk was supposed to be thin and flat, that is it does not have any tilt or warp within the optical radius; so, we looked for inclination i and position angle of the line of nodes MA for the full radius range. As a first step, we determined the position of the dynamical center and a systemic velocity suggesting a central symmetry of the velocity field. The dynamical center appears to coincide with the center of broadband isophotes with an accuracy of one pixel. The systemic velocity is found to be $2375 \text{ km} \cdot \text{s}^{-1}$ which agrees with earlier determinations (Table 1). The dispersion of systemic velocity values determined over all pairs of symmetrically taken points of the galaxy is $16 \text{ km} \cdot \text{s}^{-1}$ which is close to our accuracy of individual velocity determinations. Then we verified if the whole line-of-sight velocity field can be fitted by a pure circular rotation. The mean line-of-sight velocity residuals (r.m.s.) were calculated for 30° ranges of i and MA ; the minimum of the velocity residual calculated over the total velocity field reveals the true values of these parameters. This approach assumes that any velocity field distortions, if they exist, are of local nature.

The agreement is found the best for the following orientation parameters: $i_0 = 56^\circ$, $MA = 173^\circ$, the MA being more strictly limited and i_0 having less accuracy. If one compares these values with the photometric parameters of NGC 6181 – for example, $i = 61^\circ$ (Bottinelli et al. 1984) and $MA = 175^\circ$ (Nilson 1973) or with the data from the Table 1 – it becomes clear that the bulk of the gas in the galaxy rotates circularly.

Fig. 10 presents the azimuthally averaged rotation curve. For $r > 25''$ it is nicely flat at the level of $210 \text{ km} \cdot \text{s}^{-1}$ with an r.m.s. error of individual points not worse

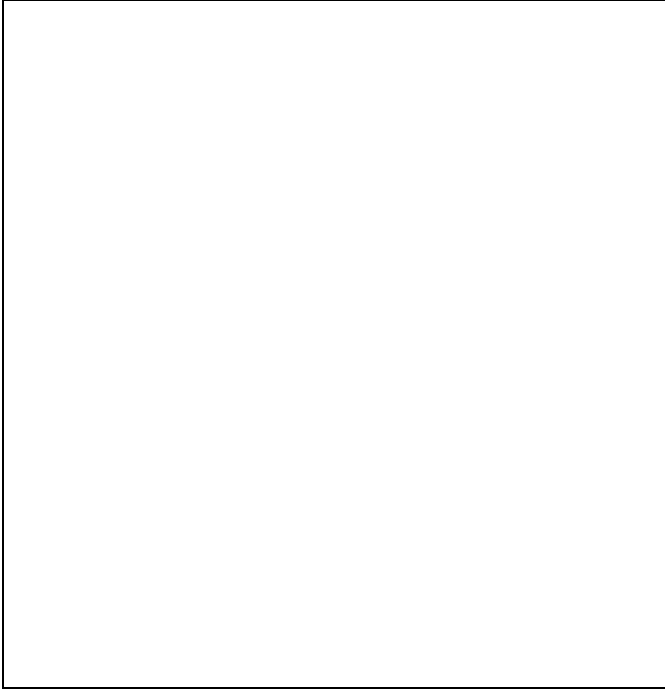


Fig. 9. Isovelocity map of NGC 6181. Velocities are in $km \cdot s^{-1}$. Cross marks the nucleus location.

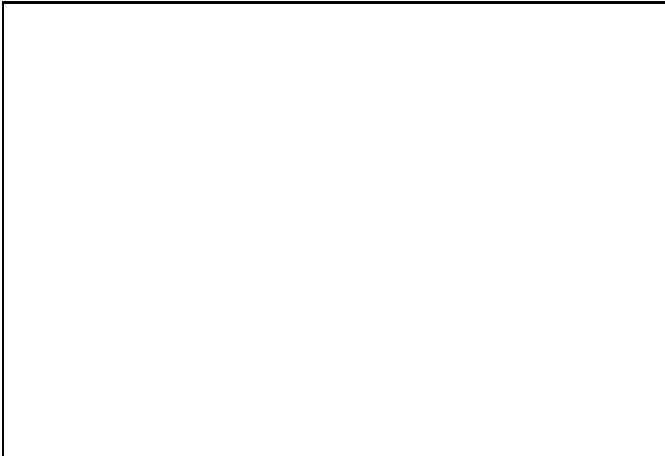


Fig. 10. Azimuthally averaged rotation curve of NGC 6181 obtained under the assumption of pure circular rotation. The inner region ($< 5''$) is excluded because of the presence of non circular motions in the center.

than $5-7 km \cdot s^{-1}$. The maximal rotation velocity estimated from the width of the HI line at 21 cm, $W50$, is $222 km \cdot s^{-1}$ (LEDA Consultation), so our rotation curve for NGC 6181 is in accordance with previously known data.

Despite the generally good accordance between the observed velocity field and the circular rotation model, there are three ranges of radial distances where essential systemic deviations from a pure circular rotation are detected with the regions of maximal deviations at $r = 30'' - 40''$

, $r \approx 12''$ and $r < 3''$. The first area is located near to the dynamical major axis and coincides neither with spiral arms nor with bright HII regions. However, the color profiles discussed in the previous section demonstrate a turnover of color radial trends at this radius. In the southern half of the galaxy this region is distinguished by the excess of azimuthal velocity of order of $30-50 km \cdot s^{-1}$, and in the northern half of the galaxy there is a similar velocity depression of about the same value. As these two areas are located symmetrically with respect to the galactic center, this anomaly may be considered rather as a kind of regular wave distortion of the velocity field than as a local velocity anomaly.



Fig. 11. Residual velocities from pure circular rotation for the inner part of the galaxy. Blank areas correspond to residual velocities between -20 and $+25 km \cdot s^{-1}$; medium blackness to -40 to $-20 km \cdot s^{-1}$; darkest regions represent positive residuals up to $+70 km \cdot s^{-1}$. The inner pair of shaded areas is related to the central mini-bar. The most remarkable extended shaded areas present the ring-like zone of radial gas motions at radius of about $10-15''$.

The model velocity field calculated in the frame of pure circular rotation with the parameters mentioned above has been subtracted from the observed velocity field. The central part of the residual velocity field is presented in Fig. 11. Here we see two halves of the ring-like region where deviations from circular rotation model locally exceed $50 km \cdot s^{-1}$. Being deprojected onto the plane of the galaxy, this region looks like three quarters of a perfect circular ring with a mean radius of $11''$ (about 1.8 kpc); the eastern half of the ring has positive residual velocities up to $55 km \cdot s^{-1}$, the western part has negative ones, from -30

to $-40 \text{ km} \cdot \text{s}^{-1}$. The width of the ring is at least 5 pixels, which corresponds to 0.8 kpc. The fact that the switching of residual velocity sign takes place near the line of nodes implies that the residual velocities here are mostly radial ones (here and below, we admit that the gas motion is in the plane of the disk). Together with a circular deprojected shape of the ring, it also gives evidences that the line of nodes of this structure is close to the MA of the global galactic disk and that the ring lies exactly in the galactic plane being purely an internal feature of the galactic gaseous subsystem. Stemming from the slightly asymmetric minor-axis surface brightness profile of the bulge one may conclude that the western half of the galactic disk is the nearest one to us. In this case we may conclude that NGC 6181 possesses a trailing spiral pattern and radially expanding gas motions in the ring.

It is worth noting that the ring of radially moving gas lies closer to the center than the beginning of the well-defined spiral arms and does not reveal itself in a brightness distribution. Nevertheless ionized gas in the ring shows systemic velocity residuals of much higher amplitude than in the bright spiral arms.

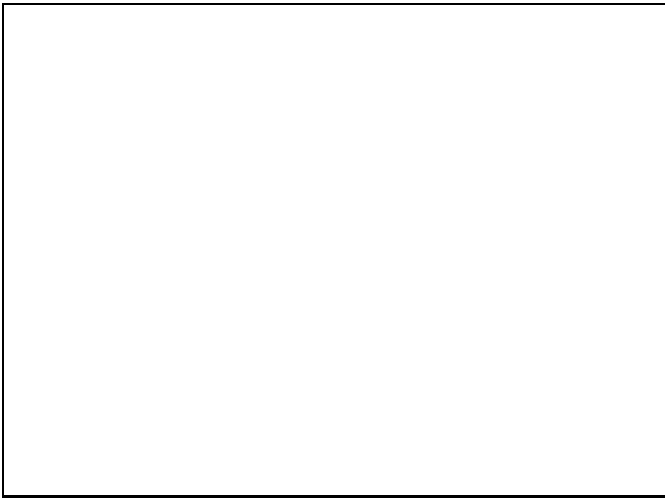


Fig. 12. Azimuthal dependence of the line-of-sight velocity central gradients within the radius range $1.8''$ – $2.2''$. The solid curve represents a cosine law fitted by a least-square algorithm.

In the very center of NGC 6181, within the region where the major axis of continuum isophotes is twisted ($r < 5''$), a clear sign of elliptical gas rotation is seen in the two-dimensional velocity field. Analysing an azimuthal dependence of central velocity gradient, we find that the maximum of the cosine curve computed by the least square approximation

$$dv_r/dr = [44.2 \cos(PA - 325.5^\circ) - 4.7] \text{ km} \cdot \text{s}^{-1} \cdot \text{arcsec}^{-1}$$

is shifted by about 30° relative to the line of nodes $MA = 173^\circ$ (Fig. 12). Hence, circumnuclear gas rotation in NGC 6181 parallel with the isophote major axis twist gives strong evidence for the presence of a small bar in the very center of the galaxy. So NGC 6181 may be applied to a small number of known galaxies where nuclear bar reveals itself both from photometric and kinematic data.

A physical connection between the central mini-bar and the ring-like zone of gas expansion may be suspected. It follows from radial velocities of gas in the ring deprojected onto the plane of the galaxy, assuming that these motions are purely radial. Parameters of the galactic plane orientation used for deprojection were taken from the best fit model of circular rotation: $i_0 = 56^\circ$, $MA = 173^\circ$. It appeared that the radial velocity of the ring expansion varies along the eastern half of the ring from 50 to $120 \text{ km} \cdot \text{s}^{-1}$ (Fig. 13), and the position angle of the maximum expansion velocity roughly coincides with the position angle of the minimum of cosine curve describing the azimuthal dependence of the central velocity gradient. It gives some evidence that the position angle of the largest radial velocities is related to the orientation of nuclear bar.

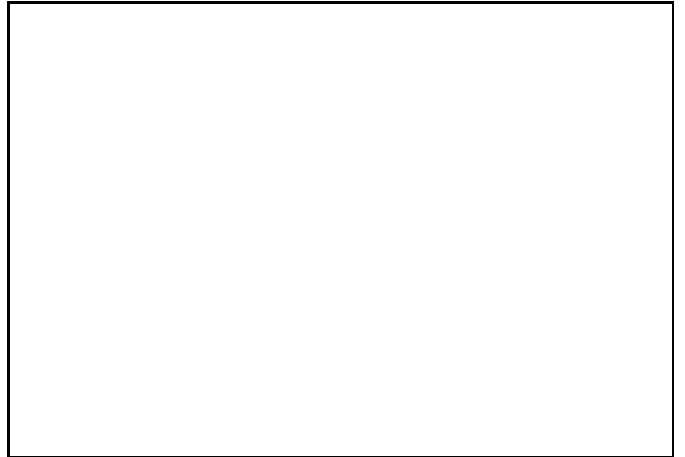


Fig. 13. Azimuthal dependence of the gas radial velocities in the ring-like zone with the radius of $12''$: residual velocities presented in Fig. 11 are deprojected onto the galactic plane under the assumption of pure radial motions with the galactic plane orientation parameters $i = 56^\circ$ and $MA=173^\circ$.

Kinematically distinct, ring-like inner regions of systemic radial motions of gas, similar to what we observe in NGC 6181, were not known yet. The only analogy, which can be mentioned, is the famous "3 kpc arm" in our Galaxy: it possesses radial velocities of about 100 – $150 \text{ km} \cdot \text{s}^{-1}$ and is probably connected with a triaxial structure of the Galactic center. The other radially expanding gaseous ring, found in NGC 4725 (Buta 1988), has a radius of 10 – 13 kpc being a structure of a quite different scale.

Note, that morphologically distinguished nuclear rings, which reveal themselves as zones of brightness, not of velocity, excess, often accompany nuclear bars (Buta & Crocker 1993). Numerical simulations confirm that gaseous subsystems may give ring-like response to a tri-axial potential form (Combes & Gerin 1985). So what we found may be considered as a kinematical counterpart of such structures as nuclear rings, related to general disk structure. In this case, as in the case of our Galaxy, it is not necessary to interpret radial gas velocities in the ring-like zone as an evidence of its real expansion due to some explosion event: there is no hint of the presence of a shock front or enhanced star formation in front of the ring or in the ring itself. A more realistic explanation is that we observe here an unusually large amplitude of hydrodynamical oscillations of gas velocities associated with the density waves which penetrate deep into the inner part of the disk (Fridman et al., in preparation).

The other feature of the velocity field of NGC 6181 is a multicomponent structure of emission line profiles in some HII regions of the disk. We performed Gauss analysis of two-component emission line profiles for the central part of the galaxy 64×64 pixels, or $45'' \times 45''$. The primary – more strong and everywhere narrow – component reveals a velocity field which excellently agrees with the field obtained in the previous analysis: a general circular rotation, elliptical gas motions in the center and ring-like zone of radial gas motions. The secondary, more weak and broad component (with gas velocity dispersion up to $200 \text{ km} \cdot \text{s}^{-1}$) appears only in the four brightest HII regions; it is absolutely absent in the ring-like zone of the radial gas motions. The difference between the "first" and the "second" velocity component averaged over the total region of the galaxy is zero, but for the bright HII region, nearest to the dynamical center, there exists a switch of velocity difference sign between the northern and the southern halves. It allows to suspect that we deal with a proper rotation of a giant star formation site.

5. Concluding remarks

Measurements of the line-of-sight velocity field for gas emission in the giant Sc galaxy NGC 6181 have allowed us to reveal some rare phenomena. The most unusual of them is the presence of a ring-like region with striking systemic deviations from the general circular rotation which may be interpreted as a strong gas radial motion. More elaborate interpretation which connects this motion with the presence of hydrodynamical 3D oscillations of gas velocities related to density wave phenomena will be given elsewhere (Fridman et al., in preparation). A small nuclear bar is also found in the galaxy both by kinematic and photometric methods.

Acknowledgements. We are very grateful to the observers of the Special Astrophysical Observatory RAS – S.N. Dodonov, S.V. Drabek, and V.V. Vlasniuk assisting us at the 6 m telescope, and

V.O. Chavushyan and S.K. Balayan which obtained the data at the 1 m telescope. During the data analysis we have used the Lyon-Meudon Extragalactic Database (LEDA) supplied by the LEDA team at the CRAL-Observatoire de Lyon (France) and of the NASA/IPAC Extragalactic Database (NED) which is operated by the Jet Propulsion Laboratory, California Institute of Technology, under contract with the National Aeronautics and Space Administration. We acknowledge also an anonymous referee for the very useful comments and advices.

References

- Afanasiev V. L., Burenkov A. N., Zasov A. V., Sil'chenko O. K., 1992, *AZh*, 69, 19
- Amram Ph., Boulesteix J., Georgelin Y.M., et al., 1991, *The Messenger*, 64, 44
- Bottinelli L., Gouguenheim L., Paturel G., de Vaucouleurs G., 1984, *A&AS*, 56, 381
- Boulesteix J., 1993, *ADHOC Reference Manual*. Marseille: Publ. de l'Observatoire de Marseille
- Boulesteix J., Georgelin Y., Marcelin M., Monnet G., 1983, *SPIE Conf. Instr. Astron.* V, 445, 37
- Burbidge E. M., Burbidge G. R., Prendergast K. H., 1965, *ApJ*, 142, 649
- Burstein D., Davies R. L., Dressler A., et al., 1987, *ApJS*, 64, 601
- Buta R., 1988, *ApJS*, 66, 233
- Buta R., Crocker D. A., 1993, *AJ*, 105, 1344
- Buta R., Williams K. L., 1995, *AJ*, 109, 543
- Combes F., Gerin M., 1985, *A&A*, 150, 327
- Elmegreen D. M., Elmegreen B. G., 1984, *ApJS*, 54, 127
- Fridman A. M., Khoruzhii O. V., Lyakhovich V. V., Sil'chenko O. K., Zasov A. V., in preparation
- Longo G., de Vaucouleurs A., 1983, *A General Catalogue of Photoelectric Magnitudes and Colors in the U, B, V System*. Austin: Univ. Texas Press
- Longo G., de Vaucouleurs A., 1985, *Supplement to the General Catalogue of Photoelectric Magnitudes and Colors of Galaxies in the U, B, V System*. Austin: Univ. Texas Press
- Neizvestny S. I., 1981, *Astrofiz. issled. Izv. SAO AS USSR*, 16, 49
- Nilson P., 1973, *Uppsala General Catalogue of Galaxies*. Uppsala Obs. Press
- Roth J., 1994, *AJ*, 108, 862
- Straizys V., 1977, *Multicolor Stellar Photometry. Photometric Systems and Methods*. Vilnius: Mokslas Publ.
- Worthey G., 1994, *ApJS*, 95, 107

This article was processed by the author using Springer-Verlag \LaTeX A&A style file *L-AA* version 3.

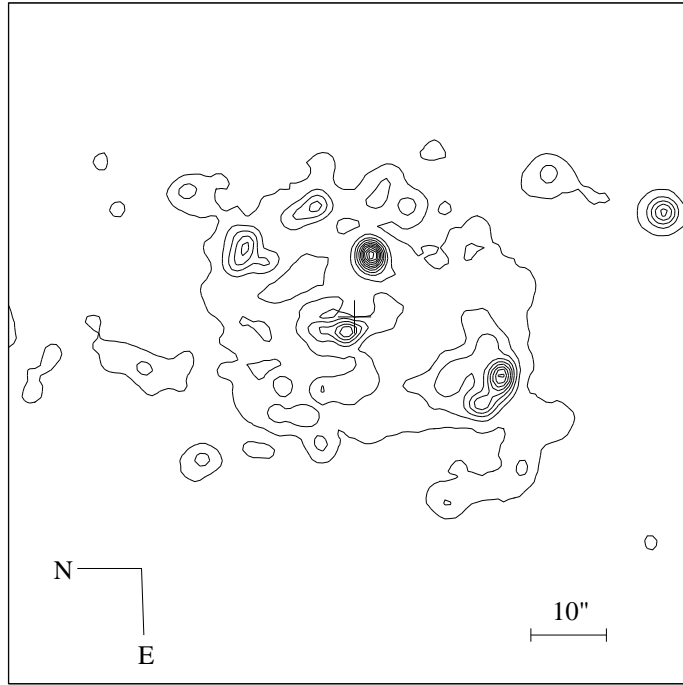
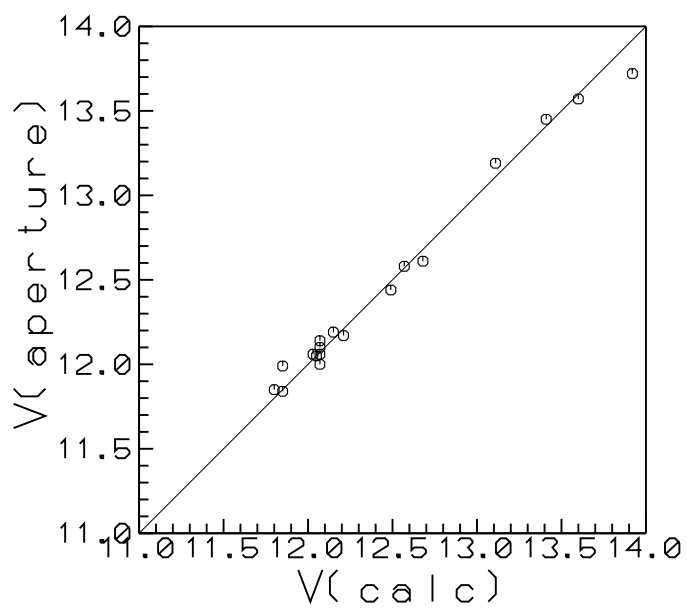
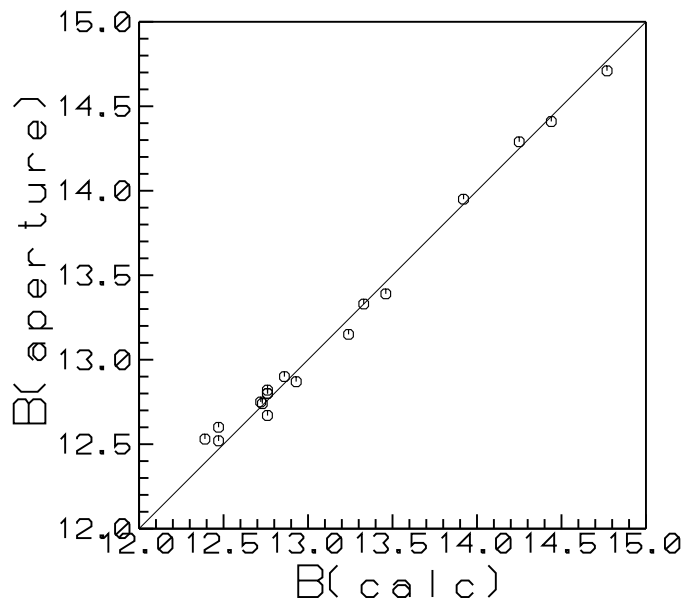


Figure 1



This figure "fig4.gif" is available in "gif" format from:

<http://arxiv.org/ps/astro-ph/9606124v1>

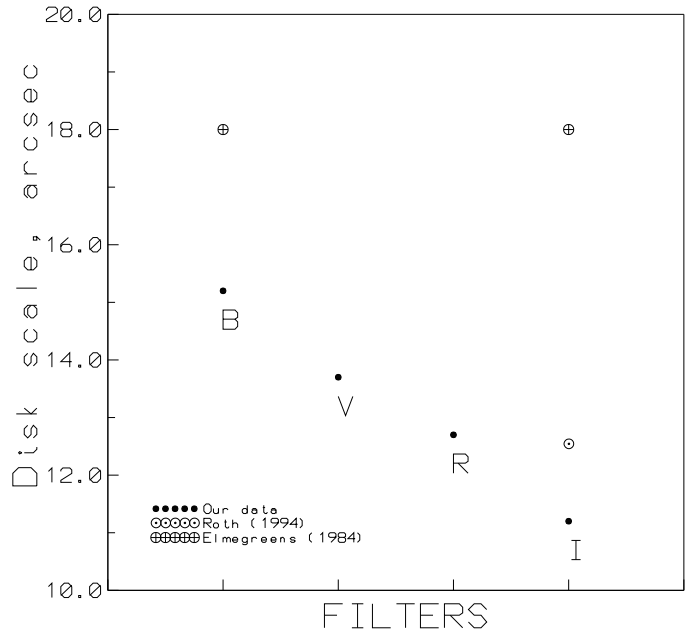


Figure 5

This figure "fig6.gif" is available in "gif" format from:

<http://arxiv.org/ps/astro-ph/9606124v1>

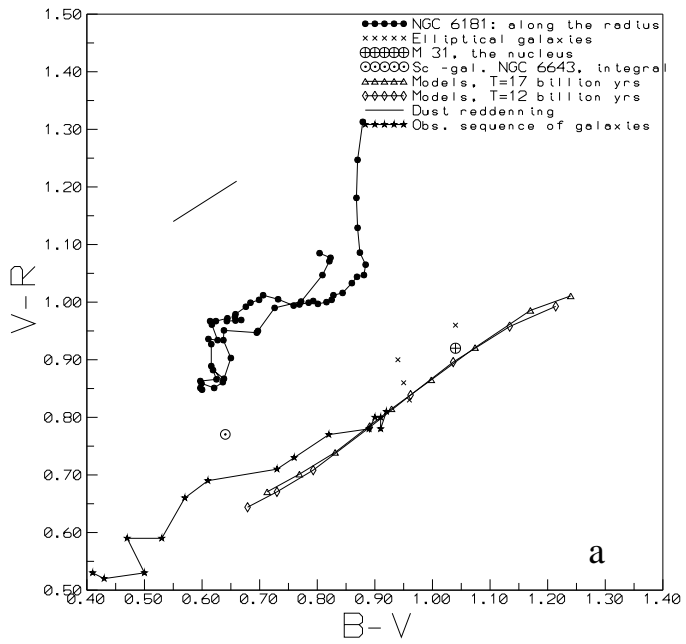
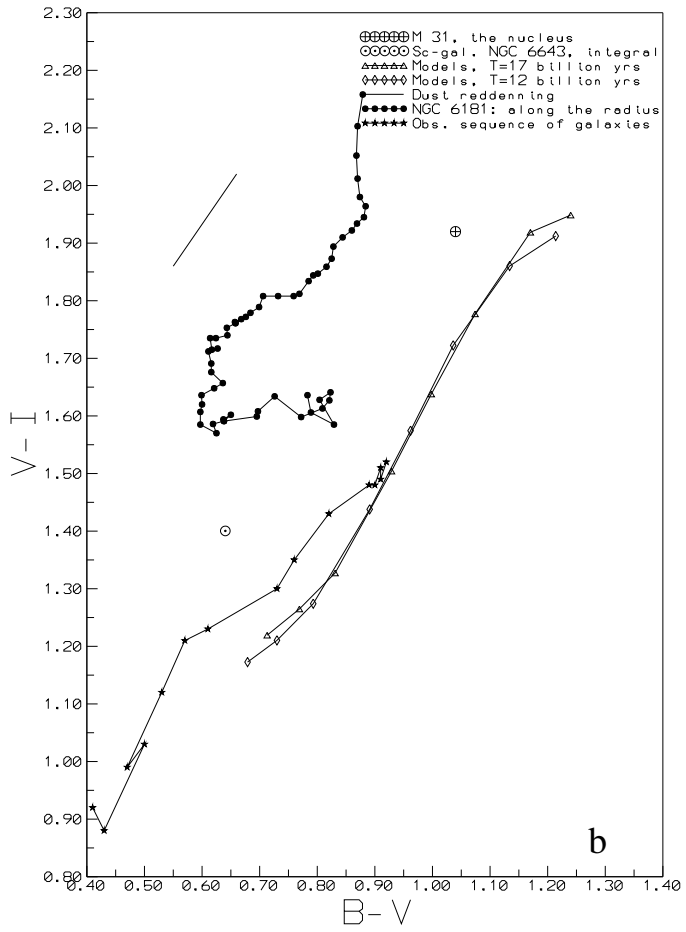
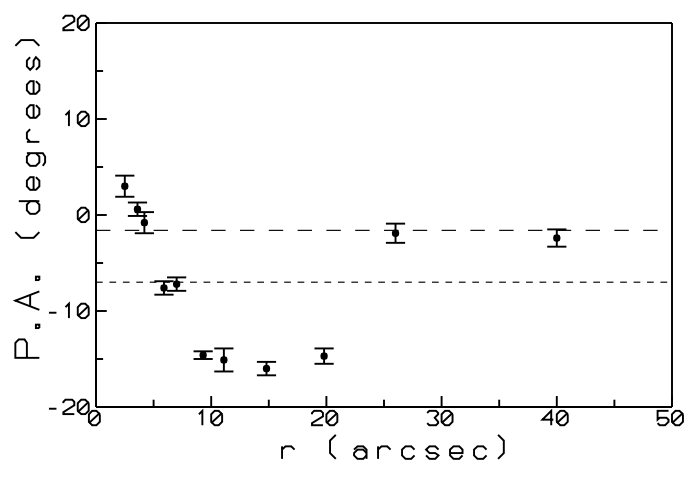


Figure 7



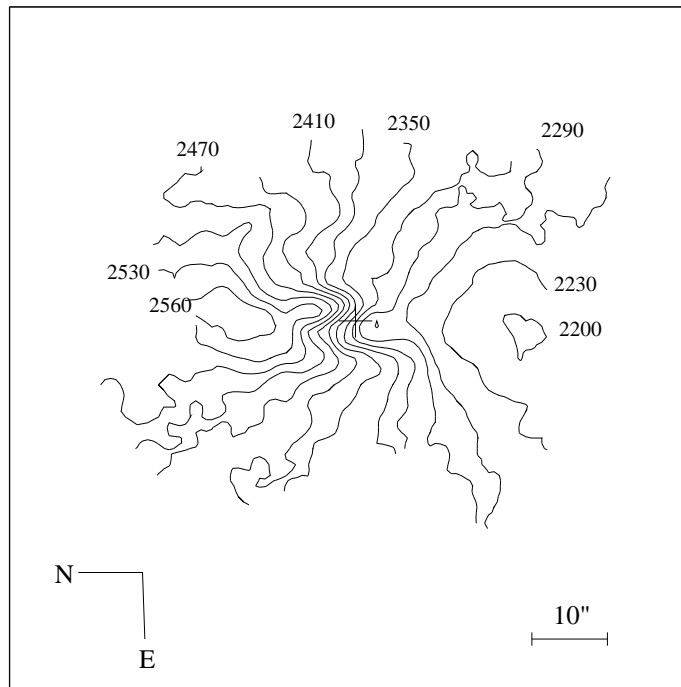


Figure 9

This figure "fig10.gif" is available in "gif" format from:

<http://arxiv.org/ps/astro-ph/9606124v1>

This figure "fig11.gif" is available in "gif" format from:

<http://arxiv.org/ps/astro-ph/9606124v1>

This figure "fig12.gif" is available in "gif" format from:

<http://arxiv.org/ps/astro-ph/9606124v1>

This figure "fig13.gif" is available in "gif" format from:

<http://arxiv.org/ps/astro-ph/9606124v1>